

Supporting Information

Nonanuclear Zinc-Gold [Zn₃Au₆] Heterobimetallic Complexes

Ravi Yadav, Milena Dahlen, Akhil K. Singh, Xiaofei Sun, Michael T. Gamer, and Peter W. Roesky*

Institute of Inorganic Chemistry, Karlsruhe Institute of Technology (KIT), Engesserstraße 15, 76131 Karlsruhe (Germany).

Email: roesky@kit.edu

Contents

1. IR Spectra	S2
2. NMR Spectra	S5
3. Single Crystal X-ray Diffraction	S12
4. Table S1: Crystal data and structure refinement.....	S13
5. Crystal Structures.....	S14
6. Photoluminescence properties.....	S18
7. Quantum chemical calculations.....	S22
8. Cartesian coordinates of the optimized structures at ground state.....	S28
9. References	S32

1. IR Spectra

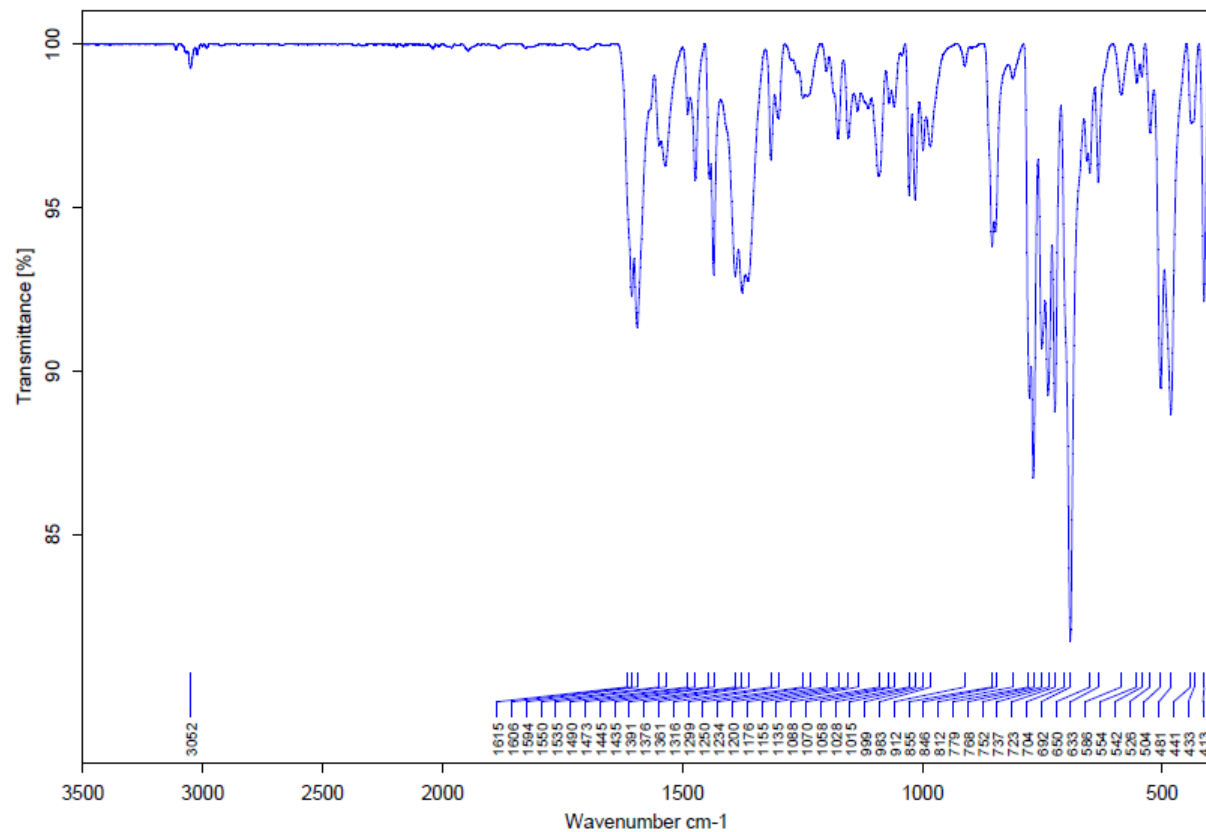


Figure S1: ATR-IR spectrum of complex **1**.

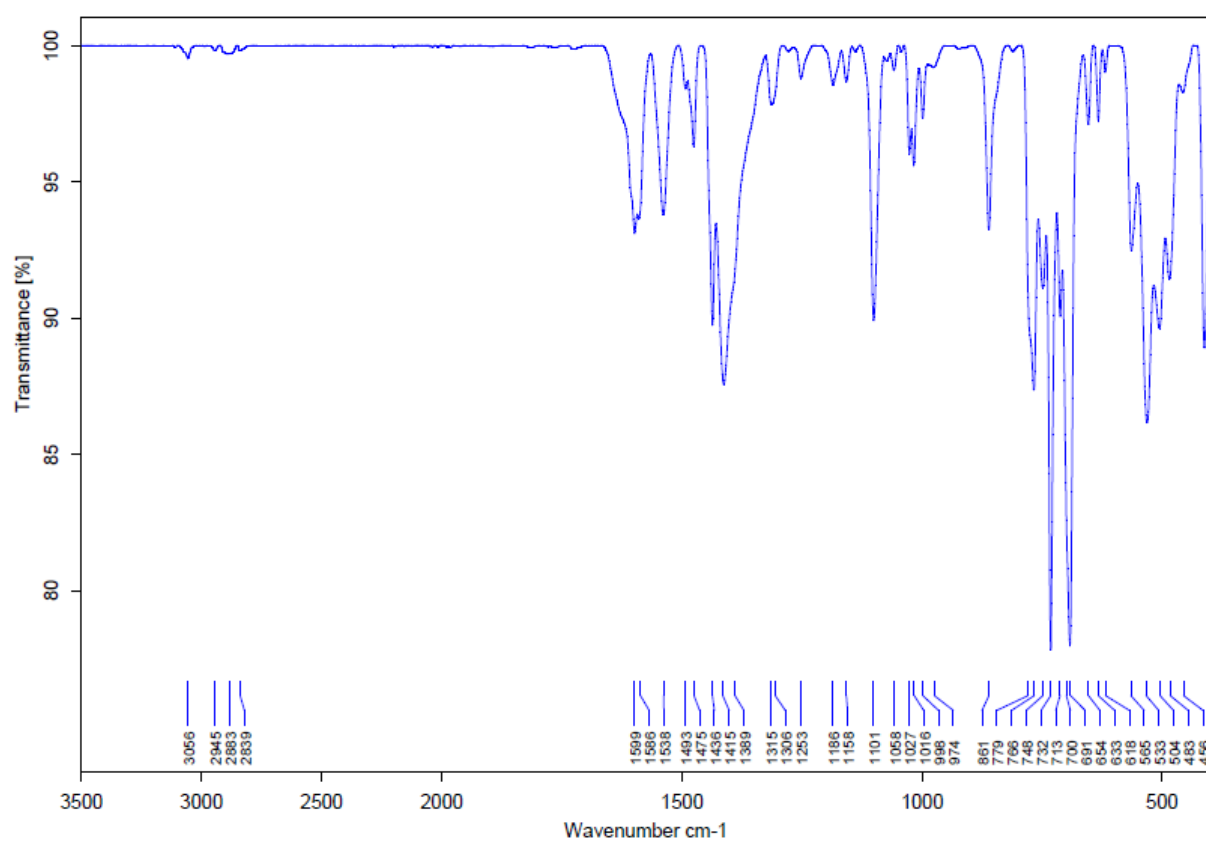


Figure S2: ATR-IR spectrum of the crude product from the reaction between **1** and $[\text{AuCl}(\text{tht})]$.

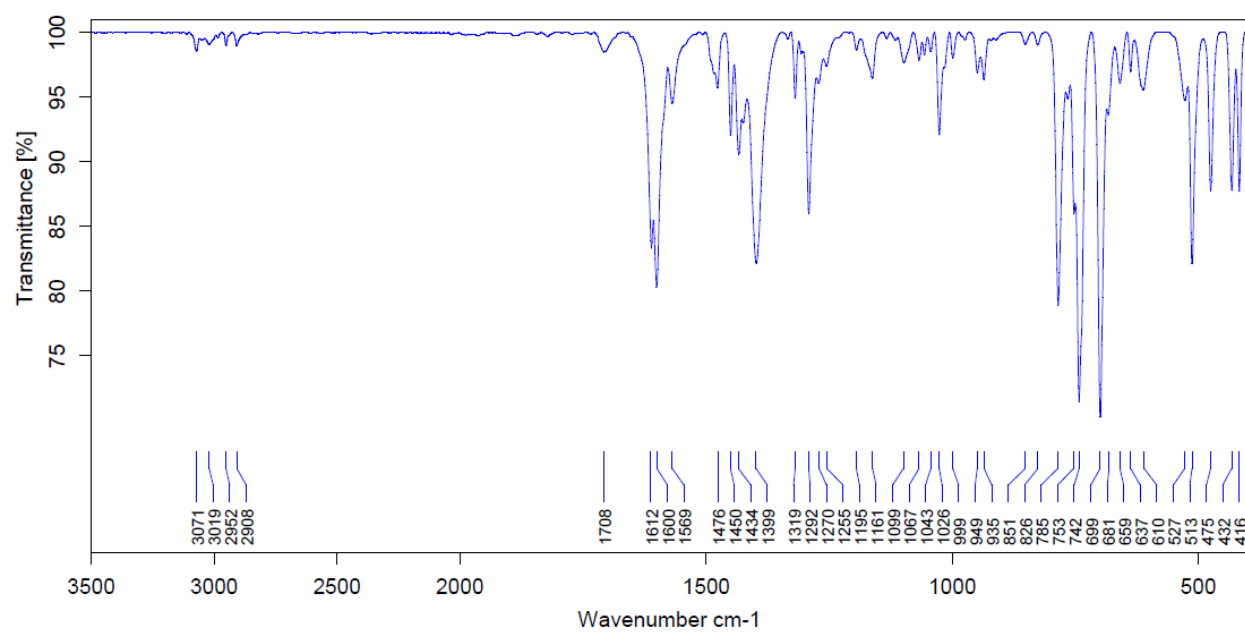


Figure S3: ATR-IR spectrum of complex 2.

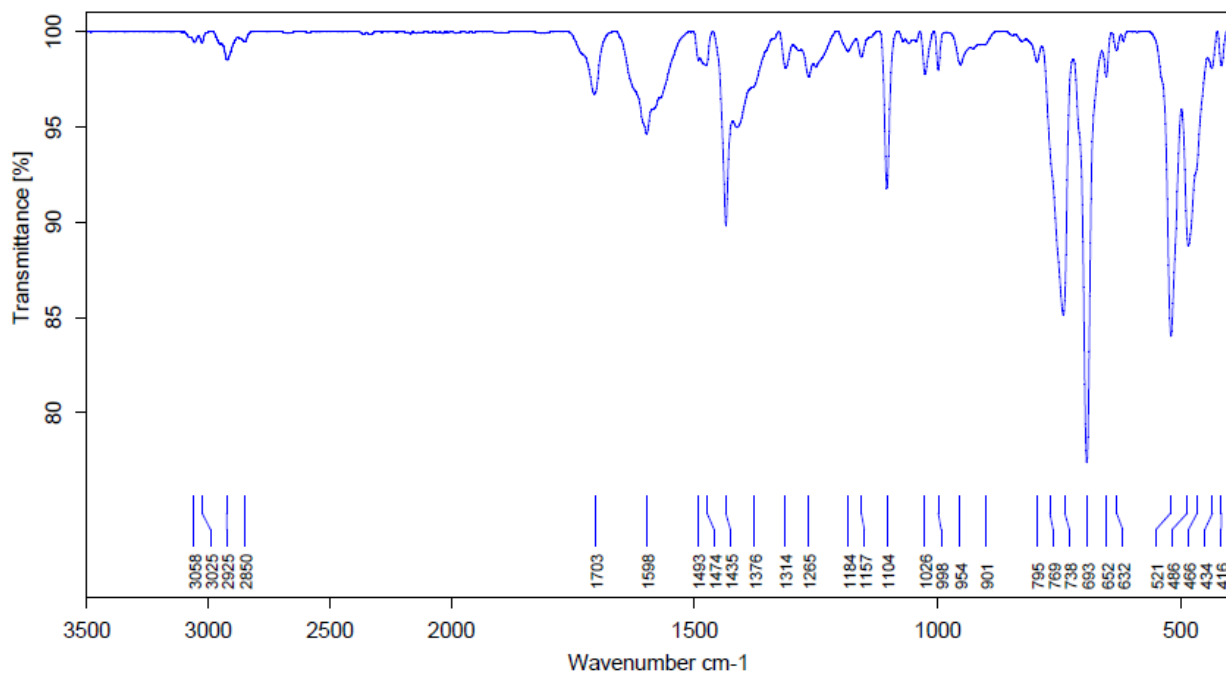


Figure S4: ATR-IR spectrum of complex 4.

2. NMR Spectra

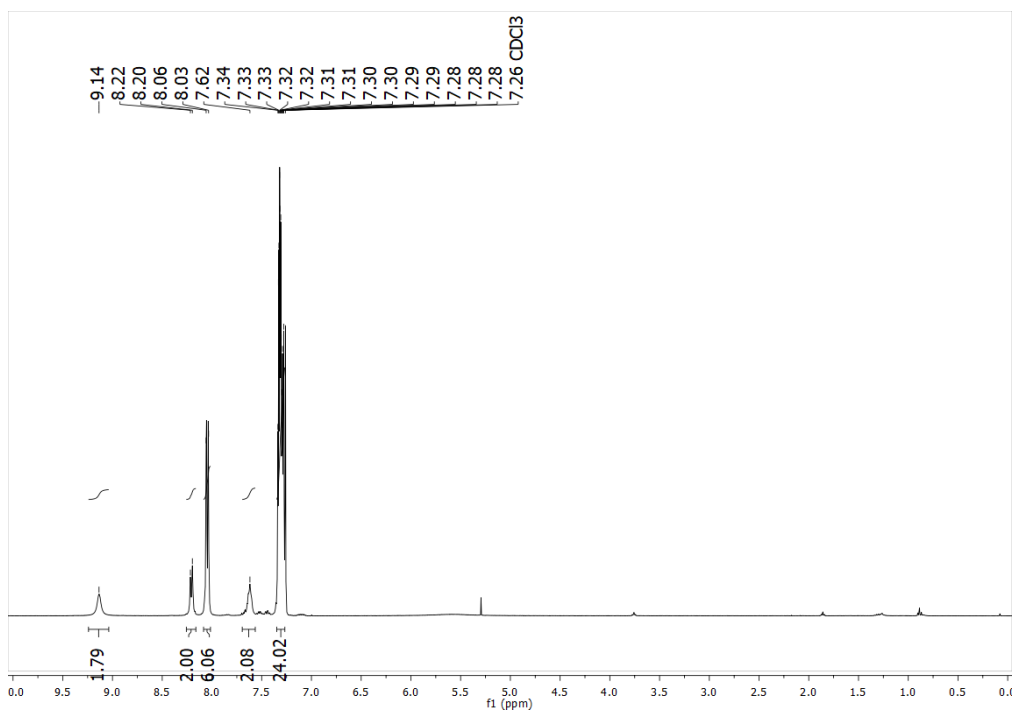


Figure S5: ^1H NMR (400 MHz, 298 K, CDCl_3) spectrum of complex **1**.

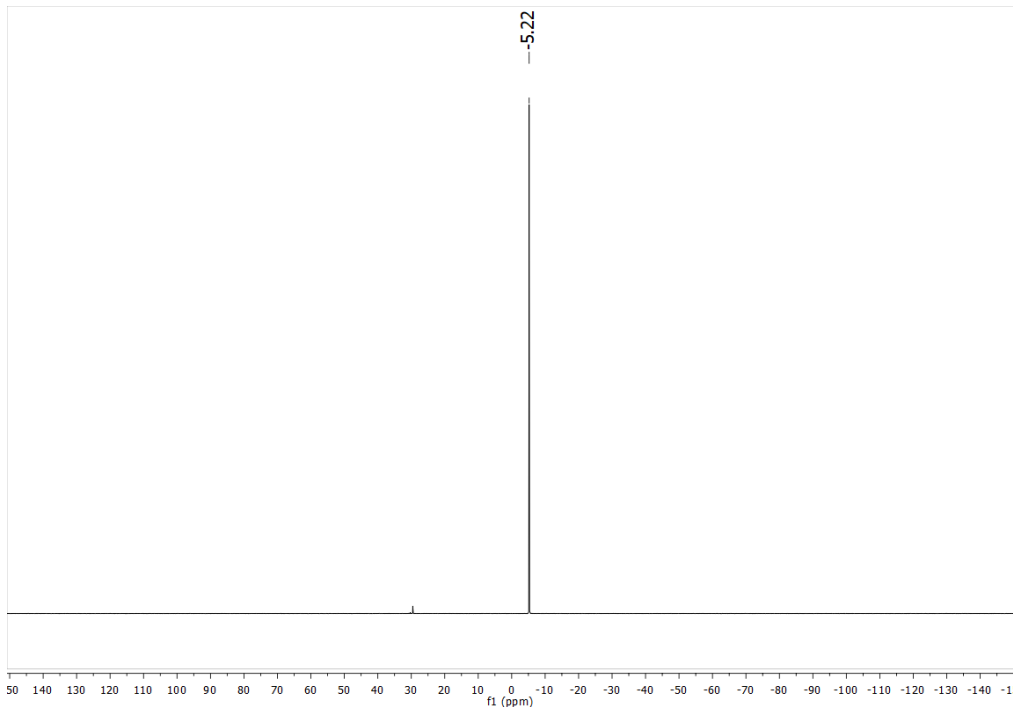


Figure S6: $^{31}\text{P}\{^1\text{H}\}$ NMR (162 MHz, 298 K, CDCl_3) spectrum of complex **1**.

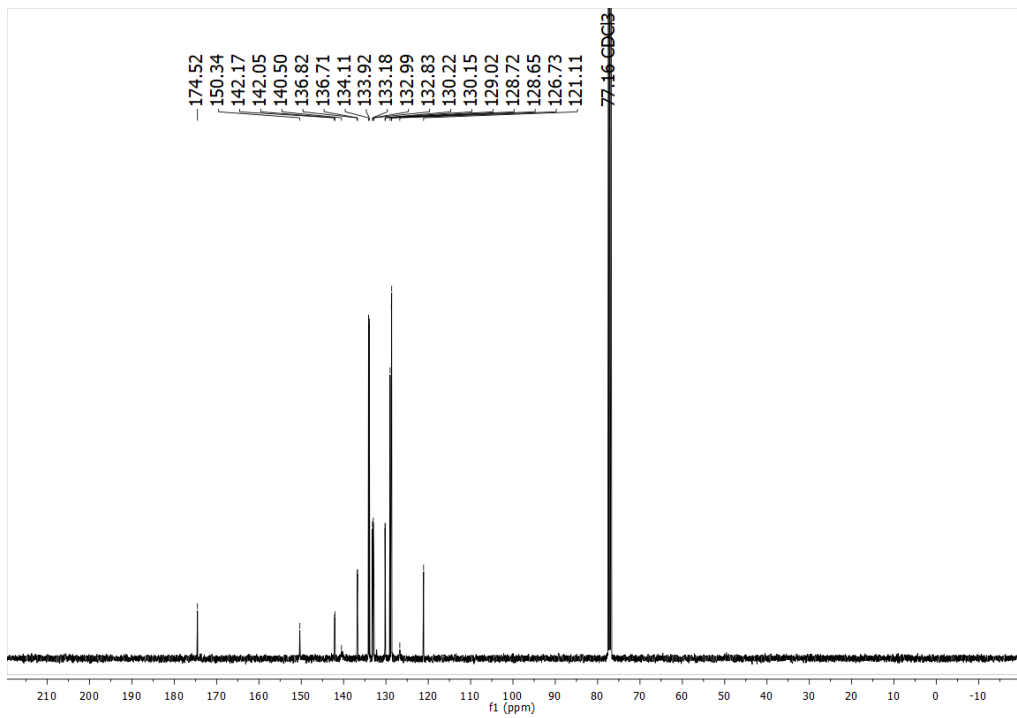


Figure S7: $^{13}\text{C}\{^1\text{H}\}$ NMR (100 MHz, 298 K, CDCl_3) spectrum of complex **1**.

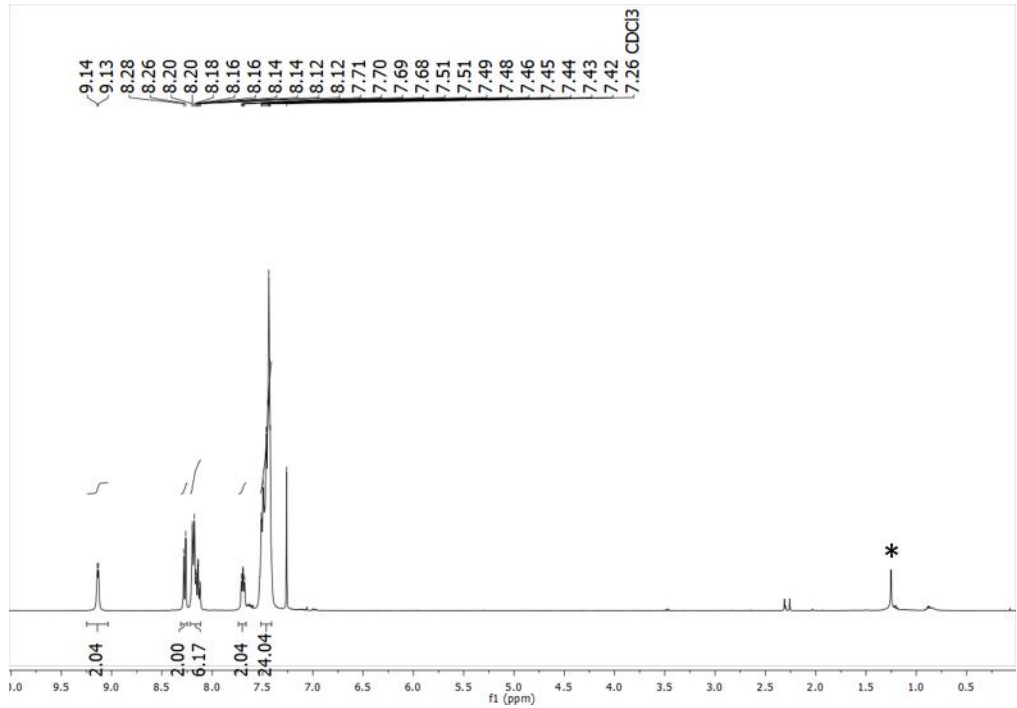


Figure S8: ^1H NMR (400 MHz, 298 K, CDCl_3) spectrum of the crude product from the reaction between **1** and $[\text{AuCl}(\text{tht})]$. (*) = H-grease.

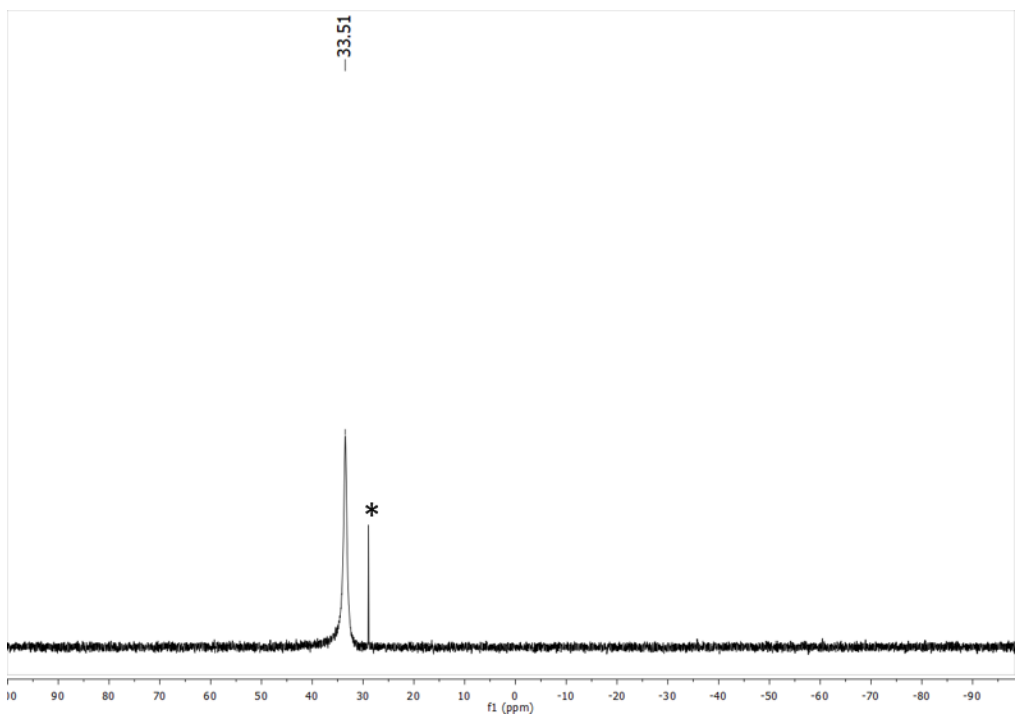


Figure S9: $^{31}\text{P}\{\text{H}\}$ NMR (162 MHz, 298 K, CDCl_3) spectrum of crude product from the reaction between **1** and $[\text{AuCl}(\text{tht})]$. Traces of an impurity due to the oxidation of phosphine of L^{Ph} (*).

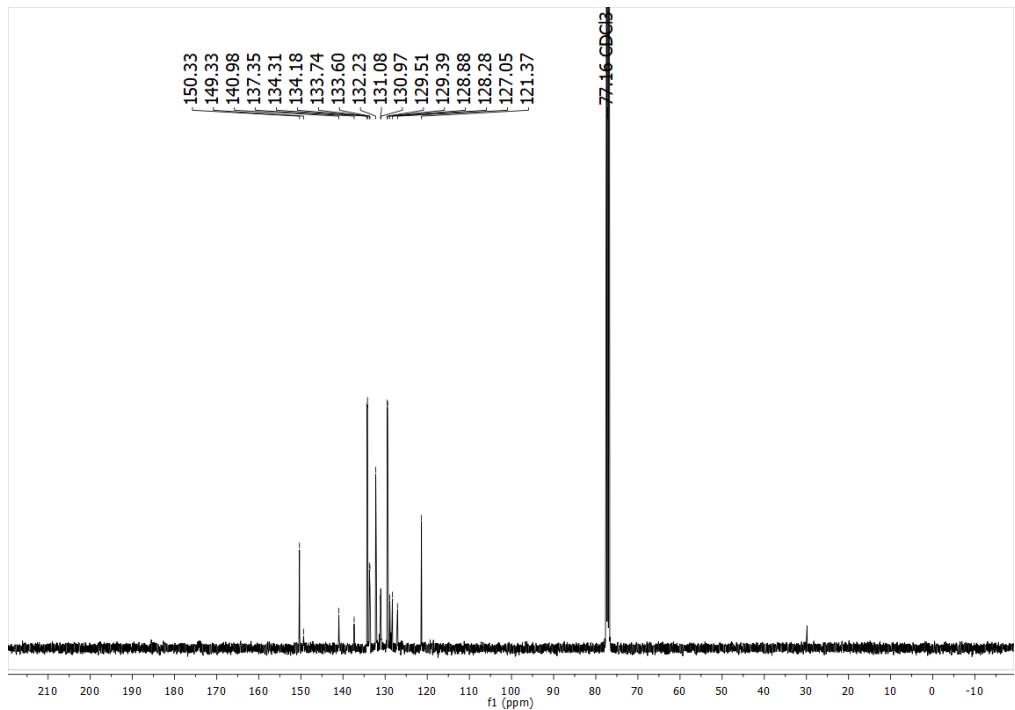


Figure S10: $^{13}\text{C}\{\text{H}\}$ NMR (100 MHz, 298 K, CDCl_3) spectrum of the crude product from the reaction between **1** and $[\text{AuCl}(\text{tht})]$.

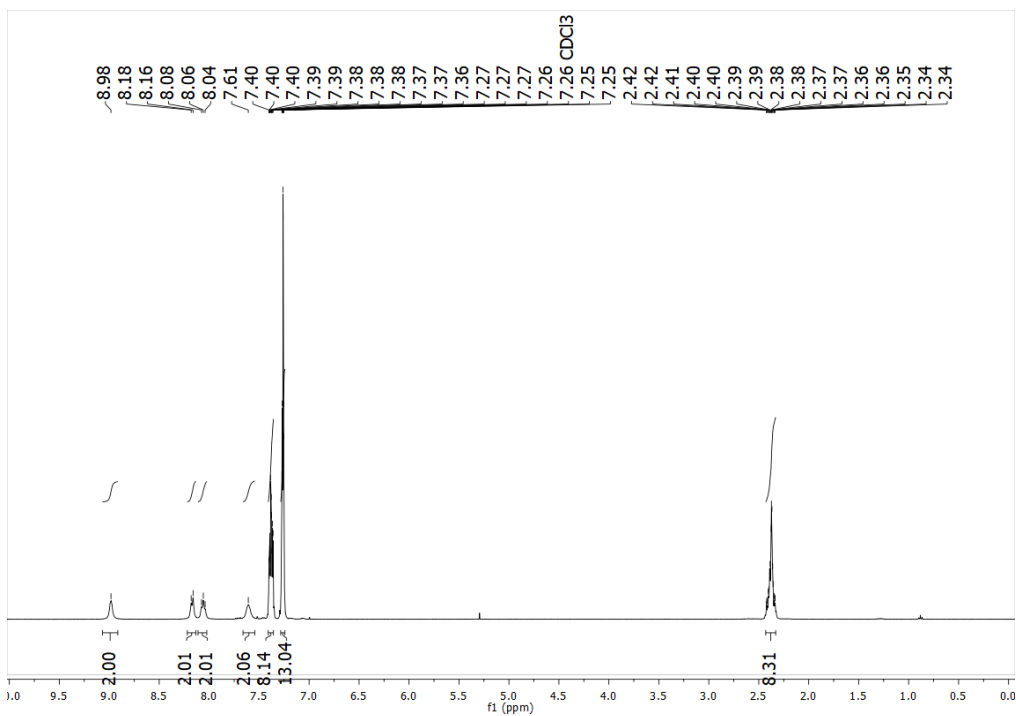


Figure S11: ^1H NMR (400 MHz, 298 K, CDCl_3) spectrum of complex 2.

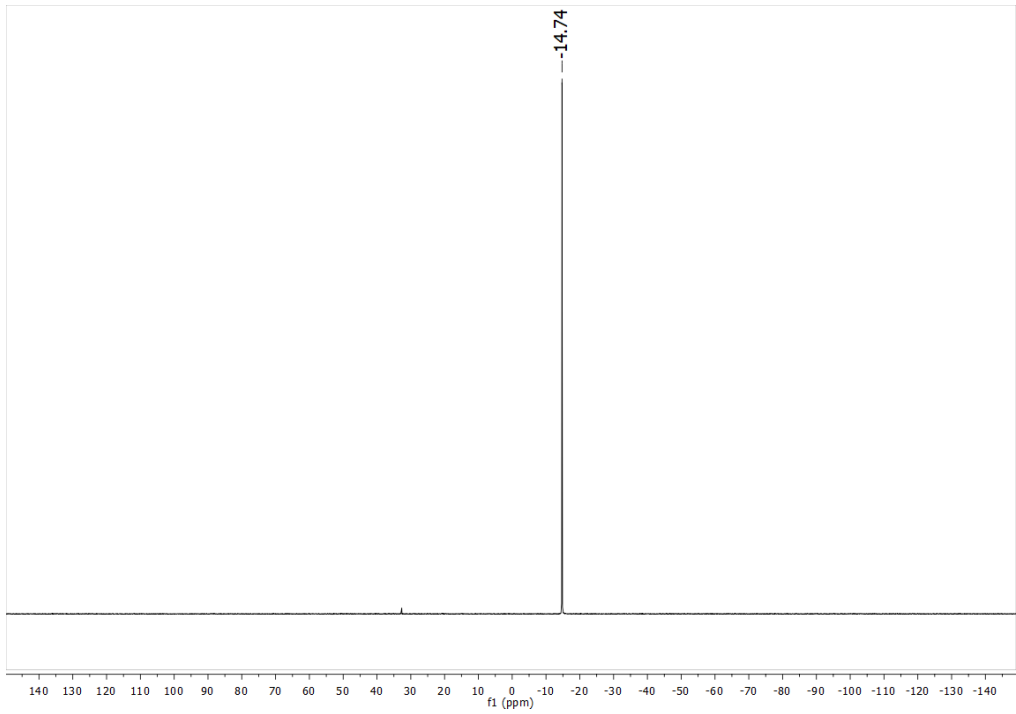


Figure S12: $^{31}\text{P}\{\text{H}\}$ NMR (162 MHz, 298 K, CDCl_3) spectrum of complex 2.

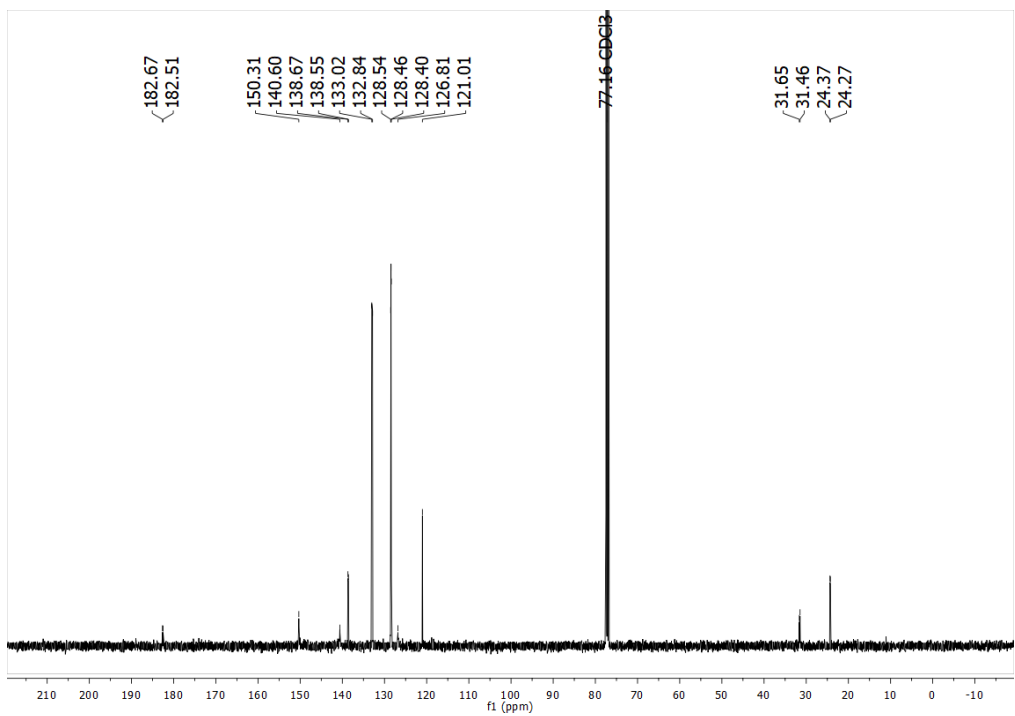


Figure S13: $^{13}\text{C}\{^1\text{H}\}$ NMR (100 MHz, 298 K, CDCl_3) spectrum of complex **2**.

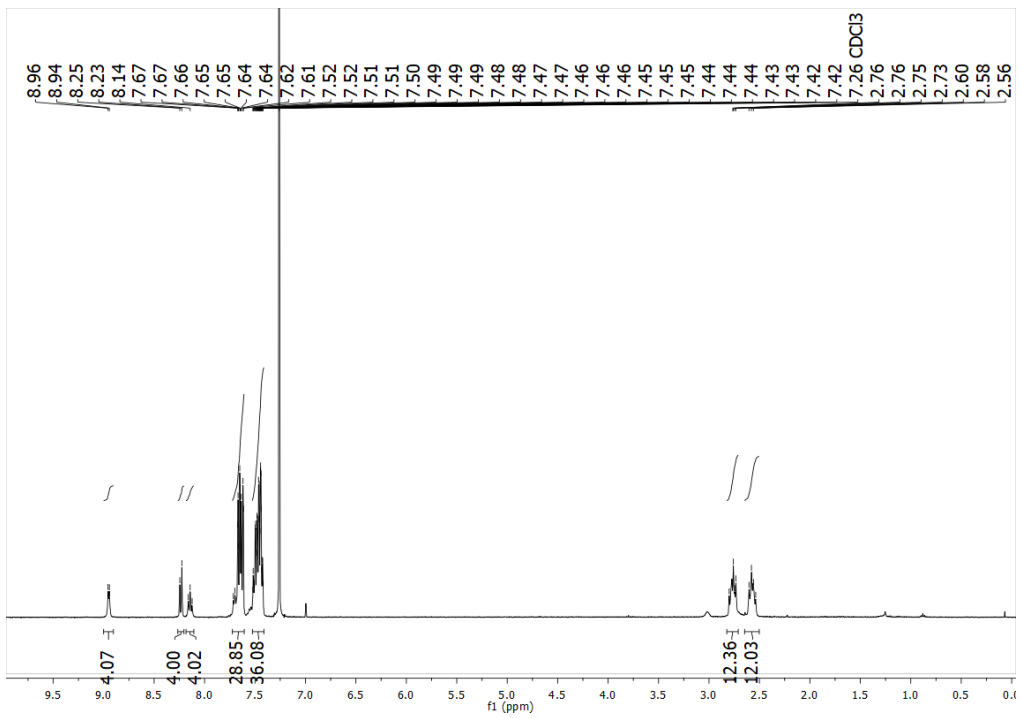


Figure S14: ^1H NMR (400 MHz, 298 K, CDCl_3) spectrum of complex **4**.

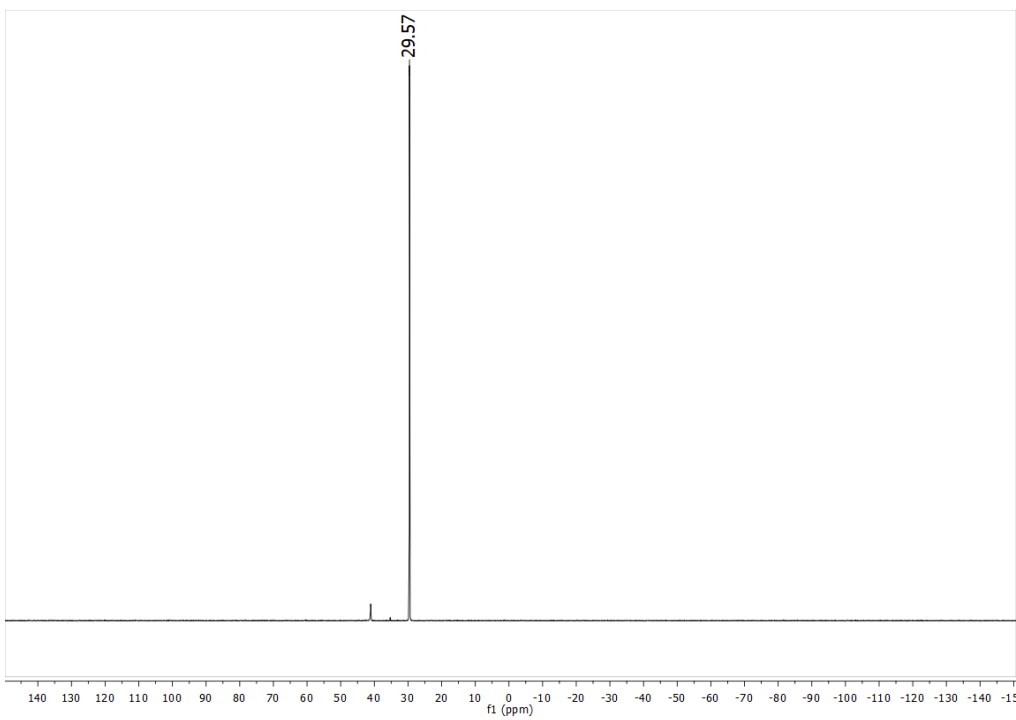


Figure S15: $^{31}\text{P}\{\text{H}\}$ NMR (162 MHz, 298 K, CDCl_3) spectrum of complex 4.

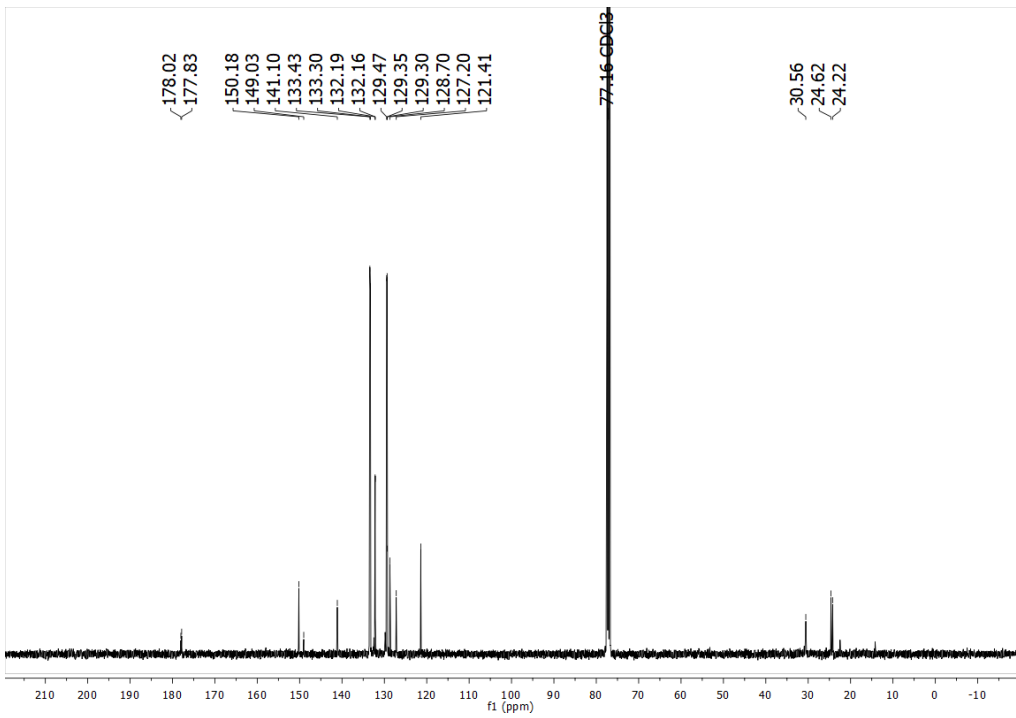


Figure S16: $^{13}\text{C}\{\text{H}\}$ NMR (100 MHz, 298 K, CDCl_3) spectrum of complex 4.

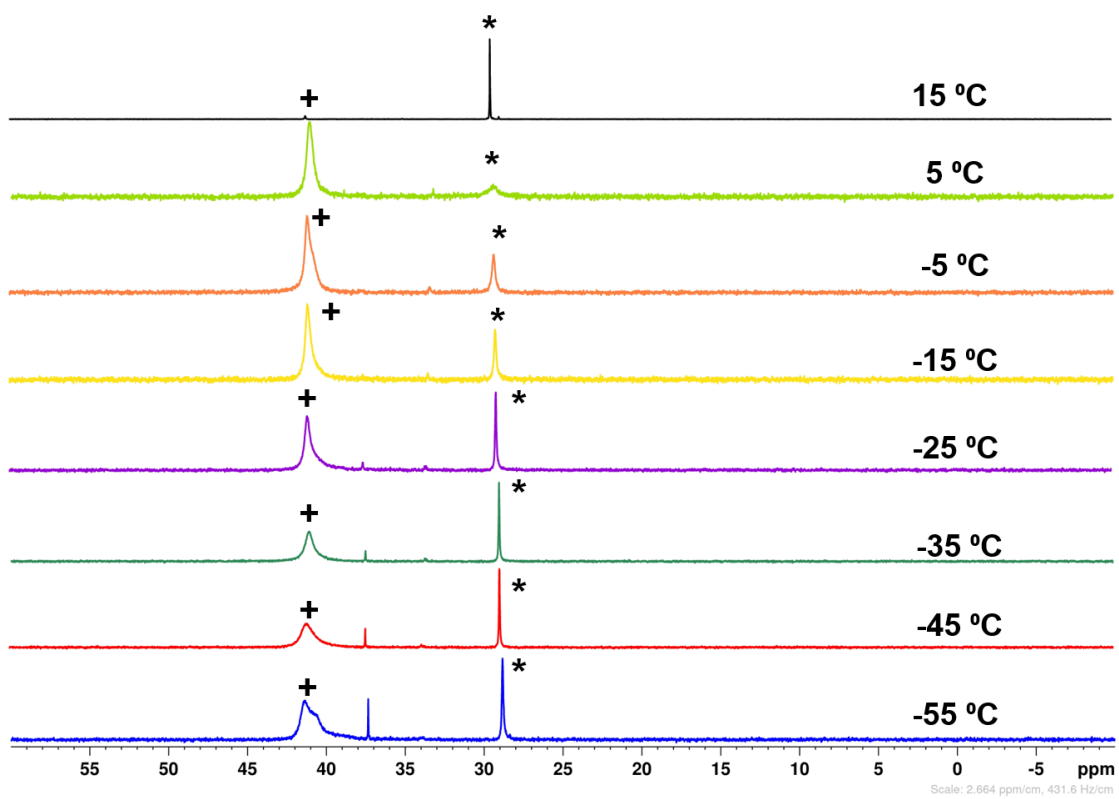


Figure S17: Stack of $^{31}\text{P}\{\text{H}\}$ NMR (162 MHz, CDCl_3) of reaction between complex **2** and $[\text{AuCl}(\text{tht})]$.

* = complex **4**, + = possible intermediate.

3. Single Crystal X-ray Diffraction

A suitable crystal was covered in mineral oil (Aldrich) and mounted on a glass fiber. The crystal was transferred directly to the cold stream of a STOE IPDS 2 or a STOE StadiVari diffractometer. All structures were solved by using the program SHELXS/T¹⁻² and Olex2.³ The remaining non-hydrogen atoms were located from successive difference Fourier map calculations. The refinements were carried out by using full-matrix least-squares techniques on F^2 by using the program SHELXL.¹⁻² In each case, the locations of the largest peaks in the final difference Fourier map calculations, as well as the magnitude of the residual electron densities, were of no chemical significance.

Crystallographic data (excluding structure factors) for the structures reported in this paper have been deposited with the Cambridge Crystallographic Data Centre as a supplementary publication number 2051757-2051760. Copies of the data can be obtained free of charge on application to CCDC, 12 Union Road, Cambridge CB21EZ, UK (fax: +(44)1223-336-033; email: deposit@ccdc.cam.ac.uk).

Refinement Details

Complex **3** has positive residual electron density (8.43×10^{-3}) which is due to crystals are slightly twinned, but neither Stoe Twin Integration nor manual search for suitable twin law were successful. Problem seems to be caused by a disordered Ph₂PAuCl group, at which a phenyl group switches place with the AuCl moiety at est. 4-5%. So only the electron density of the disordered gold atom can be located, which causes the error. Due to low intensity compared to the Au atom, modelling of the remaining disordered group failed.

Complex **4** have disordered non-coordinating thf molecules which could not be modeled satisfactorily and were therefore removed from the electron density map using the Olex2 solvent mask routine.³

4. Table S1: Crystal data and structure refinement.

Compound	1	2	3	4
Formula	C ₄₈ H ₃₆ N ₂ O ₄ P ₂ Zn	C ₄₀ H ₃₆ N ₂ O ₄ P ₂ Zn	C ₁₃₄ H ₁₀₀ Au ₆ Cl ₆ N ₄ O ₁₂ P ₆ Zn ₃	C ₁₁₀ H ₁₀₀ Au ₆ Cl ₆ N ₄ O ₁₂ P ₆ Zn ₃
D _{calc.} / g cm ⁻³	1.380	1.359	1.820	1.769
μ/mm ⁻¹	0.741	0.815	7.197	10.453
Formula Weight	832.10	736.02	3734.60	3446.36
Colour	colourless	colourless	colourless	colourless
Shape	block	plate	prism	block
Size/mm ³	0.46×0.39×0.29	0.36×0.20×0.05	0.20×0.13×0.06	0.07×0.05×0.03
T/K	150	100	100	180
Crystal System	triclinic	orthorhombic	triclinic	triclinic
Space Group	P-1	Aea2	P-1	P-1
a/Å	10.3183(5)	26.0998(8)	11.1558(5)	13.2692(3)
b/Å	14.3647(8)	17.2345(4)	17.0682(7)	16.5355(3)
c/Å	15.5865(8)	7.9957(2)	19.4466(8)	16.8719(3)
α/°	110.168(4)		67.913(3)	106.060(2)
β/°	101.993(4)		84.830(3)	104.914(2)
γ/°	103.328(4)		83.908(3)	104.036(2)
V/Å ³	2003.08(19)	3596.60(16)	3406.6(3)	3235.46(12)
Z	2	4	1	1
Z'	1	0.5	0.5	0.5
Wavelength/Å	0.71073	0.71073	0.71073	1.34143
Radiation type	Mo K _α	Mo K _α	Mo K _α	Ga K _α
Θ _{min} /°	1.599	2.489	2.264	2.881
Θ _{max} /°	29.217	29.490	29.642	63.999
Measured Refl.	20291	33626	31566	34599
Independent Refl.	10736	4327	16242	15365
Reflections with I > 2(I)	8854	4051	13536	13813
R _{int}	0.0150	0.0302	0.0266	0.0267
Parameters	514	222	823	664
Restraints	0	1	192	0
Largest Peak	0.549	1.255	8.431	1.923
Deepest Hole	-0.310	-0.438	-3.259	-2.207
GooF	1.043	1.017	1.045	1.059
wR ₂ (all data)	0.0819	0.0951	0.1651	0.1174
wR ₂	0.0785	0.0929	0.1581	0.1157
R ₁ (all data)	0.0403	0.0382	0.0702	0.0422
R ₁	0.0303	0.0351	0.0591	0.0399

5. Crystal Structures

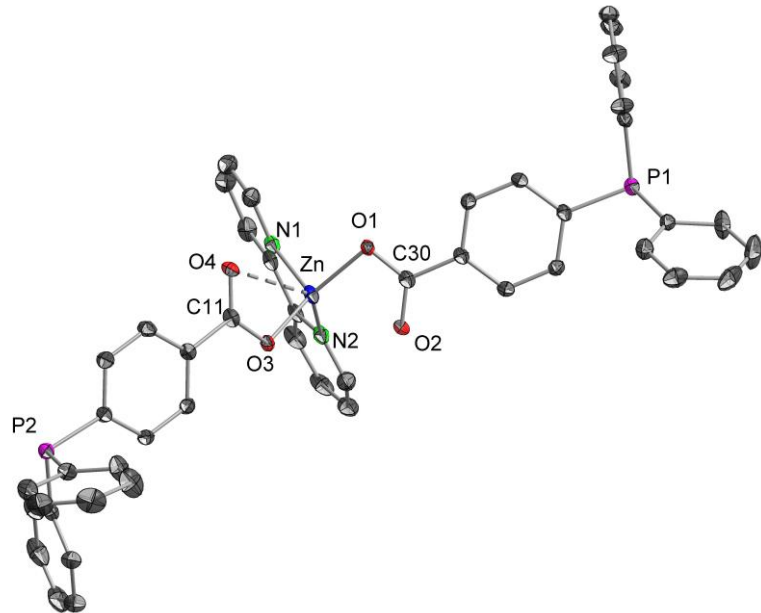


Figure S18: Molecular structure of **1** in the solid state with thermal ellipsoids at the 40% probability. H atoms and non-coordinating solvent molecules are omitted for clarity. Selected bond distances (\AA) and angles [$^\circ$]: Zn-N1 2.0667(12), Zn-O1 1.9207(10), Zn-N2 2.0868(12), Zn-O3 1.9809(10), Zn-O4 2.4785(11), O1-C11 1.2873(2), O2-C11 1.231(2), O3-C30 1.275(2), O4-C30 1.240(2); O1-Zn-O3 127.40(5), O1-Zn-O4 101.73(4), O3-Zn-O4 57.73(4), O3-Zn-O4 57.73(4), O2-C11-O1 123.72(13), O4-C30-O3 121.73(13).

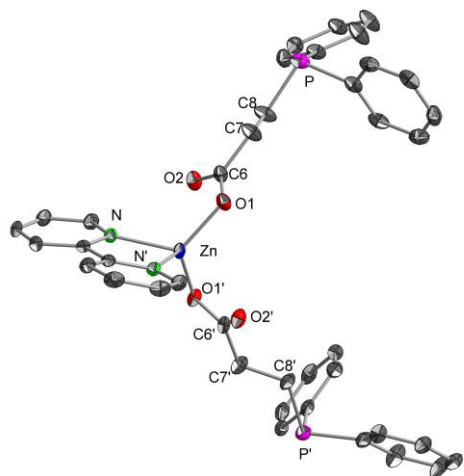


Figure S19: Molecular structure of **2** in the solid state with thermal ellipsoids at the 40% probability. H atoms and non-coordinating solvent molecules are omitted for clarity. Selected bond distances (\AA) and angles [$^\circ$]: Zn-N 2.056(3), Zn-O1 1.939(2), O1-C6 1.286(4), O2-C6 1.235(4); O1-Zn-O1' 118.3(2), N-Zn-N' 79.7(2), O2-C6-O1 122.5(3).

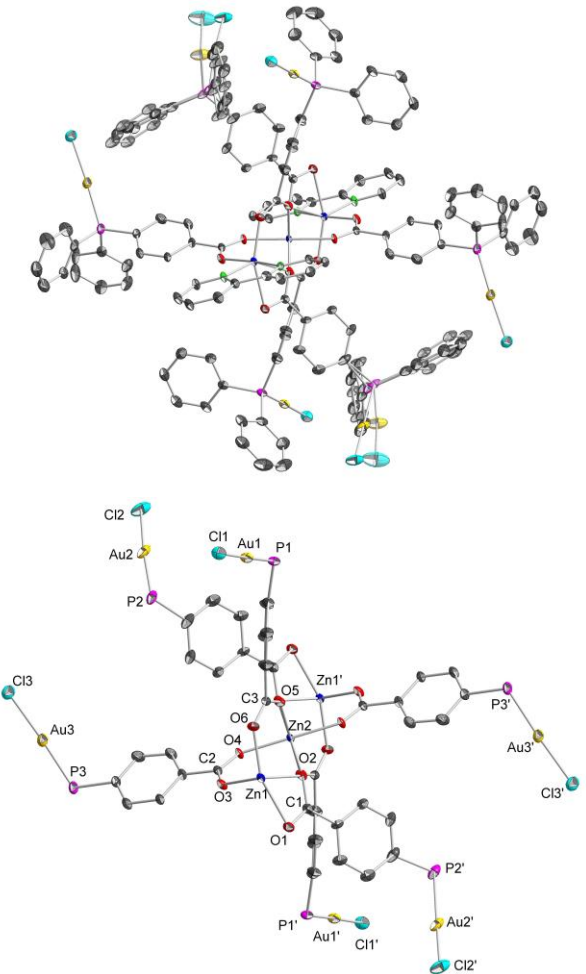


Figure S20: Left: molecular structure of complex **3** in the solid state with thermal ellipsoids at the 40% probability. Right: molecular structure of complex **3** with omitted, bipyridines and phenyl groups for clarity. Hydrogen atoms are omitted for clarity. Selected bond lengths (\AA) and angles [$^\circ$]: Au1-Cl1 2.283(2), Au2-Cl2- 2.27(2), Au3-Cl3 2.296(3), Au1-P1 2.220(2), Au2-P2 2.16(2), Au3-P3 2.224(2), Zn1-O1 2.279(6), Zn1-O2 2.137(5), Zn1-O3 2.022(5), Zn1-O6 2.029(5), Zn1-N1 2.114(6), Zn1-N2 2.159(6), Zn1-C1 2.535(7), Zn2-O2 2.182(5), Zn2-O2 2.182(5) Zn2-O4 2.068(5), Zn2-O4 2.068(5), Zn2-O5 2.053(5), Zn2-O5 2.053(5), O1-C1 1.228(9), O2-C1 1.290(9), O3-C2 1.255(9), O4-C2 1.253(8), O5-C3 1.250(9), O6-C3 1.263(9); P1-Au1-Cl1 178.97(8), P2-Au2-Cl2 169.9(8), P3-Au3-Cl3 177.34(9), O1-C1-O2 121.2(7), O4-C2-O3 127.5(7), O5-C3-O6 126.3(6).

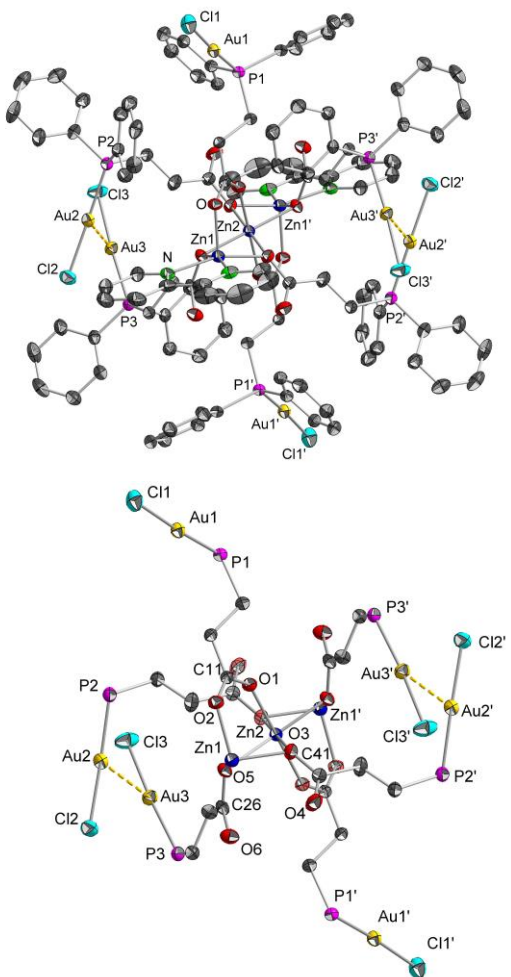


Figure S21: Left: molecular structure of complex **4** in the solid state with thermal ellipsoids at the 40% probability. Right: molecular structure of complex **4** with omitted, bipyridines and phenyl groups for clarity. Hydrogen atoms are omitted for clarity. Selected bond lengths (\AA) and angles [$^\circ$]: Au2-Au3 3.3512(3), Au1-Cl1 2.2810(11), Au2-Cl2 2.2845(11), Au3-Cl3 2.2903(12), Au1-P1 2.2308(9), Au2-P2 2.2346(9), Au3-P3 2.2404(10), Zn1-O1 2.003(3), Zn1-O3 2.177(3), Zn1-O5 2.150(2), Zn2-O2 1.994(3), Zn2-O3 2.056(3), Zn2-O5 2.053(3), Zn2-N1 2.137(3), Zn2-N2 2.108(4), O1-C11 1.268(4), O2-C11 1.249(4), O3-C41 1.298(5), O4-C41 1.206(5), O5-C26 1.300(5), O6-C26 1.222(5); P1-Au1-Cl1 175.61(4), P2-Au2-Cl2 172.80(5), P3-Au3-Cl3 175.05(5), O2-C11-O1 126.1(3), O6-C26-O5 124.1(3), O4-C41-O3 123.3(4).

6. Photoluminescence properties

All investigation of the photoluminescence (PL) properties were carried out under inert atmosphere. The samples were therefore sealed in a “Young” NMR tube (material Suprasil® quartz glass) using above mentioned glove box. As cooling agent for low temperature measurements liquid nitrogen (77 K) was used with the sample being placed directly within it. All emission and excitation spectra were recorded on a PTI QuantaMaster™ 8075-22 fluorometer with each double excitation and emission monochromators (HORIBA Jobin Yvon GmbH). For emission detection, a PMT detector R928 photomultiplier (HORIBA Jobin Yvon GmbH) in the range of 250 nm – 800 nm was used. All spectra were corrected for the wavelength dependent response of the detector and the spectrometer. For detection of the emission decay traces, the sample was excited with either a Delta Diode™ (HORIBA Jobin Yvon GmbH, Model DD-370, $\lambda_{\text{Exc}} = 370$ nm, pulse width 800 ps) for fluorescence lifetimes or a PTI XenonFLash™ (set before the emission monochromators, frequency 300 MHz) for phosphorescence decay times. For determination of the lifetimes the obtained traces were fit with an exponential decay curve using Origin(Pro) (Version 2019. OriginLab Corporation, Northampton, MA, US). Please note: The experimental setup has a detection limit of ~2 ns. In case of detected lifetimes close to this value the actual lifetime is expected to be <2 ns and cannot be determined more accurately. Same limitation applies to lifetimes in the single digit microsecond range (~6 µs) due to the maximum frequency of used Xenon flash lamp. Lifetimes determined ~6 µs are most likely to belong to a faster decay which cannot be resolved using this setup. Therefore, an assignment whether a lifetime actually is ~6 µs or if it is a much shorter lifetime (perhaps already determined with the DeltaDiode) and which simply can't be displayed, cannot be performed.

Table S2: PL decay traces of solid complexes **1** and **2** excited with a ns-pulsed LED diode at 370 nm at the depicted wavelengths and temperatures. Traces were recorded at indicated emission wavelengths. The decay traces were fit with mono-exponential/ bi-exponential curves.

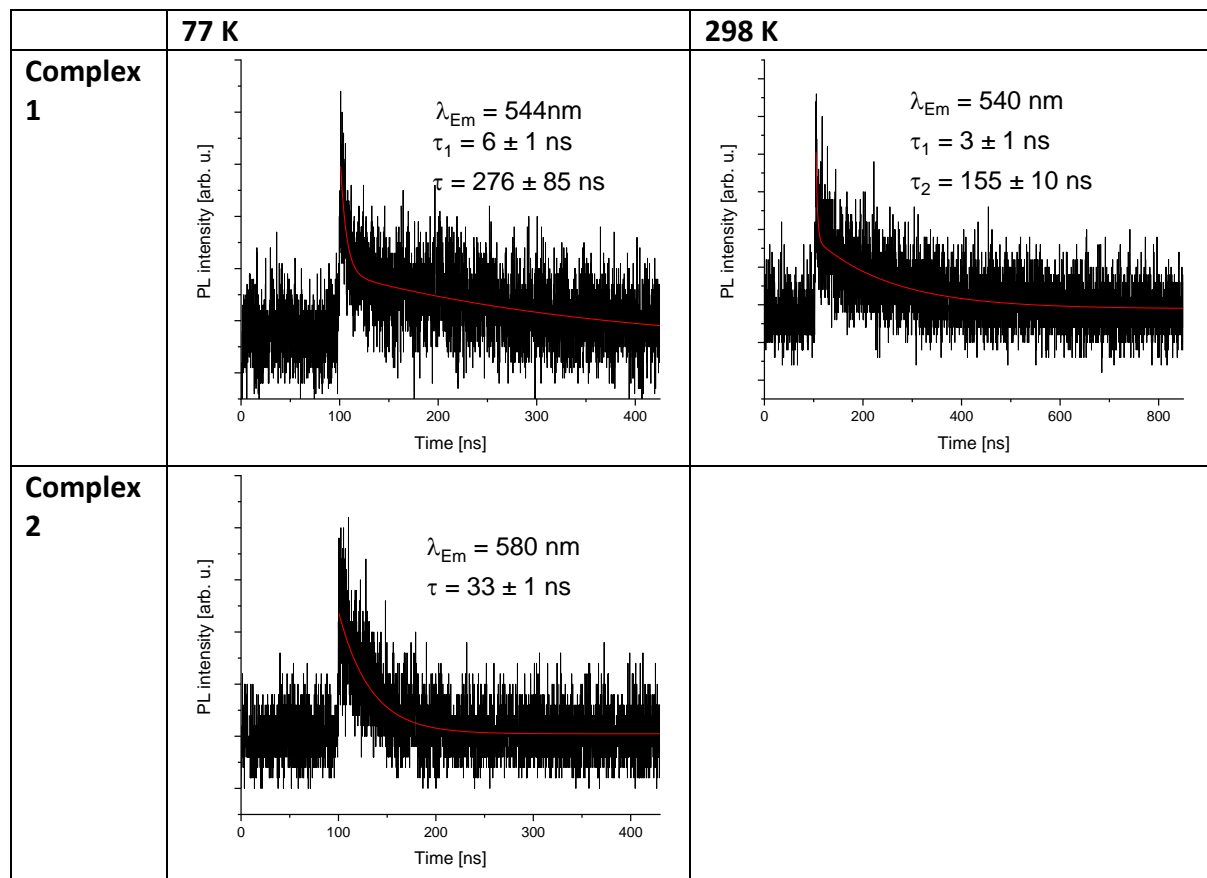
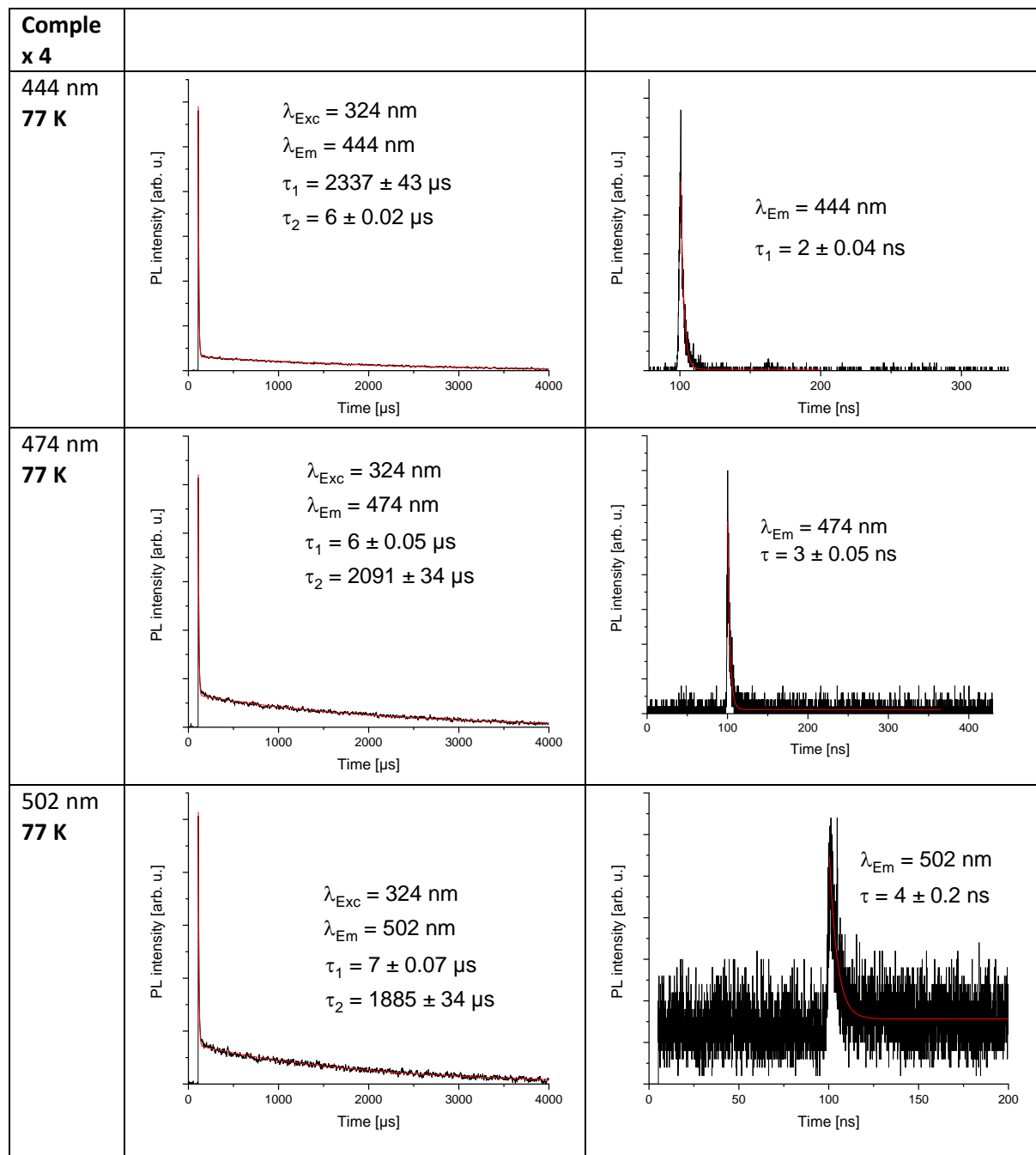
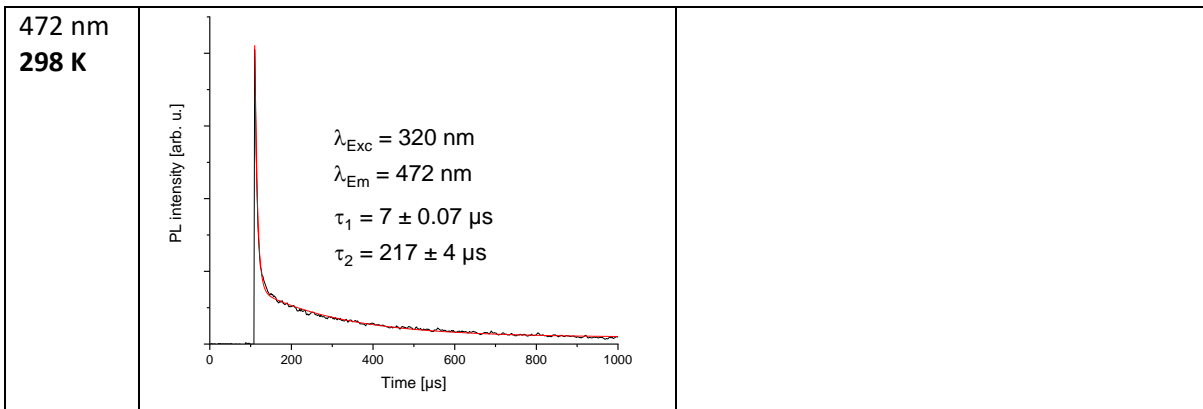


Table S3: PL decay traces of solid complex **4** excited with a ns-pulsed LED diode at 370 nm or with a Xenon flash lamp at the depicted wavelengths and temperatures. Traces were recorded at indicated emission wavelengths. The decay traces were fit with mono-exponential/ bi-exponential curves.





7. Quantum chemical calculations

The ground state geometry optimizations were initiated from the coordinates taken from the crystal structure coordinates of complexes **1**, **2** and **4**. All structure optimizations were carried out using the *Gaussian 16, revision C.01, package*.⁴ The geometry optimizations have been done without any constraints and frequency calculations were also performed on all the optimized geometries to ensure that the optimized geometries did not have any imaginary frequencies. Vertical excitation has been performed on ground state geometry. Based on the vertical excitation, suitable excited states were also optimized to assign emission bands. Geometry optimizations have been carried out using the unrestricted density functional method CAM-B3LYP⁵ functional which was proven to be good for long range excitation analysis. The basis set was DEF2SVP for gold atom, LANL2DZ for Zn atom and 6-31G** for C, P, O and H atoms. The complexes **1**, **2** and **4** were optimized as a charge neutral species with a spin multiplicity of singlet. The complex **4** was also optimized with spin multiplicity of triplet to assign phosphorescence bands. The assignment of emission bands were successfully carried out (Table S4). Visualization of the molecular orbitals and the corresponding diagrams were done employing the Chemcraft software.⁶

Table S4. Vertical absorption and emission energies E (eV), wavelengths λ (nm), of complexes **1**, **2** and **4** with TD-DFT/CAM-B3LYP level.

Absorption					Emission			
Complex	ES	E	λ	configuration	ES	E	λ	configuration
1	S1	3.09	400	HOMO-15→LUMO HOMO-15→LUMO+1 HOMO-27→LUMO+2	S1	2.17	571	HOMO→LUMO+2 HOMO-2→LUMO+2
	S2	3.29	377	HOMO→LUMO+3 HOMO-1→LUMO+3 HOMO-3→LUMO+3 HOMO-2→LUMO+14	S2	3.09	400	HOMO-15→LUMO HOMO-15→LUMO+1
	S3	3.29	377	HOMO-1→LUMO+3 HOMO→LUMO+4 HOMO-2→LUMO+14	S3	3.29	377	HOMO-1→LUMO+4 HOMO-4→LUMO+4 HOMO-5→LUMO+13
2	S1	3.10	401	HOMO-14→LUMO HOMO-14→LUMO+1 HOMO-20→LUMO	S1	1.76	702	HOMO-6→LUMO HOMO-5→LUMO
	S2	3.45	359	HOMO-1→LUMO+5 HOMO-1→LUMO+6 HOMO→LUMO+5 HOMO→LUMO+5 HOMO→LUMO+6	S2	3.45	359	HOMO-1→LUMO+5 HOMO-1→LUMO+6 HOMO→LUMO+5
	S3	3.45	359	HOMO→LUMO+5 HOMO-1→LUMO+6 HOMO-1→LUMO+3	S3	3.45	359	HOMO-1→LUMO+5 HOMO-1→LUMO+6 HOMO→LUMO+5
4	S1	3.08	402	HOMO-24→LUMO HOMO-24→LUMO+1 HOMO-27→LUMO HOMO-27→LUMO+1	S1			
	S2	3.08	402	HOMO-24→LUMO HOMO-25→LUMO HOMO-26→LUMO HOMO-27→LUMO	S2			
	S3	3.48	356	HOMO-10→LUMO+5 HOMO-11→LUMO+6 HOMO-6→LUMO+6	S3			
	T1	1.50	826	HOMO-49→LUMO HOMO-50→LUMO	T1			
	T2	1.86	665	HOMO-66→LUMO HOMO-40→LUMO	T2			

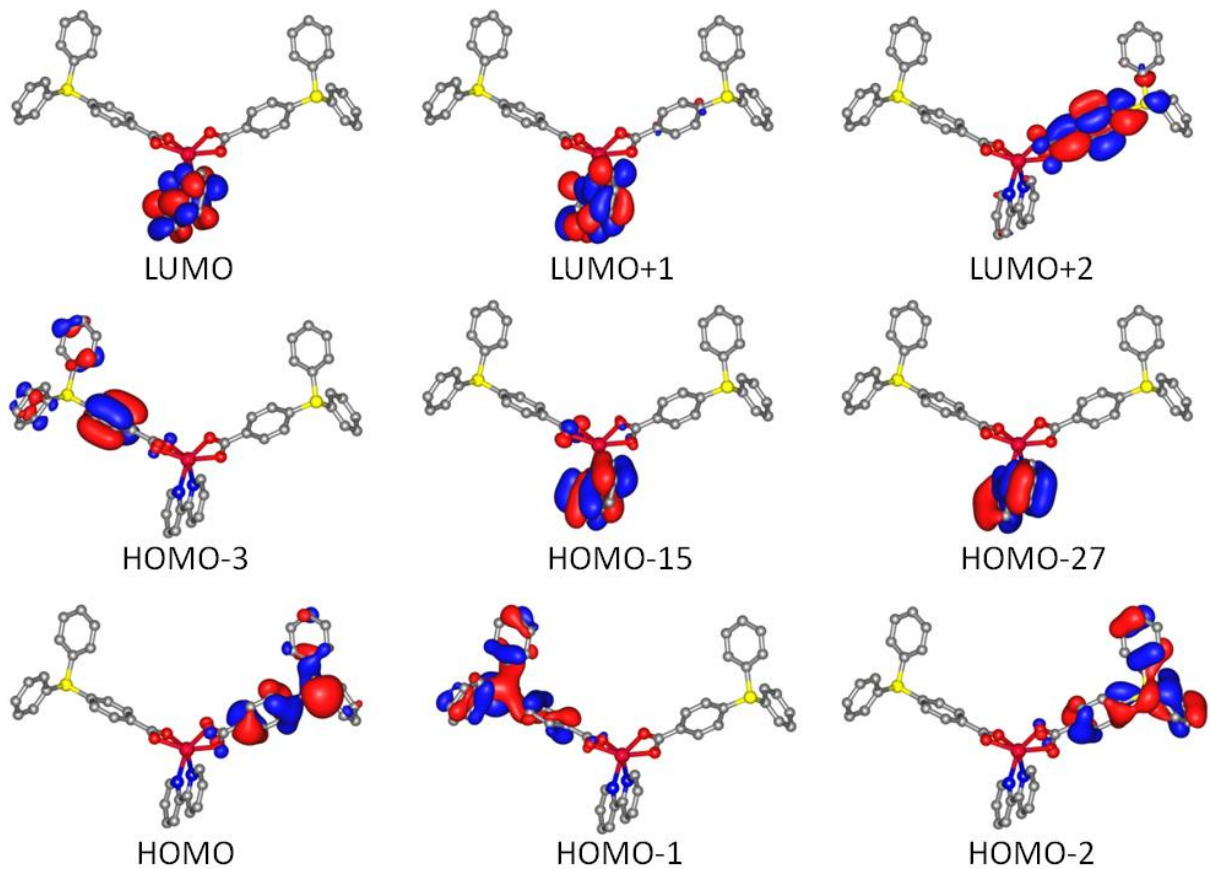


Figure S22: Molecular orbitals involved in the leading electronic configurations associated with the lowest energy $S_0 \rightarrow S_1$, S_2 , S_3 transitions in complex **1**. The MO surfaces are plotted at an isosurface value of 0.03 au.

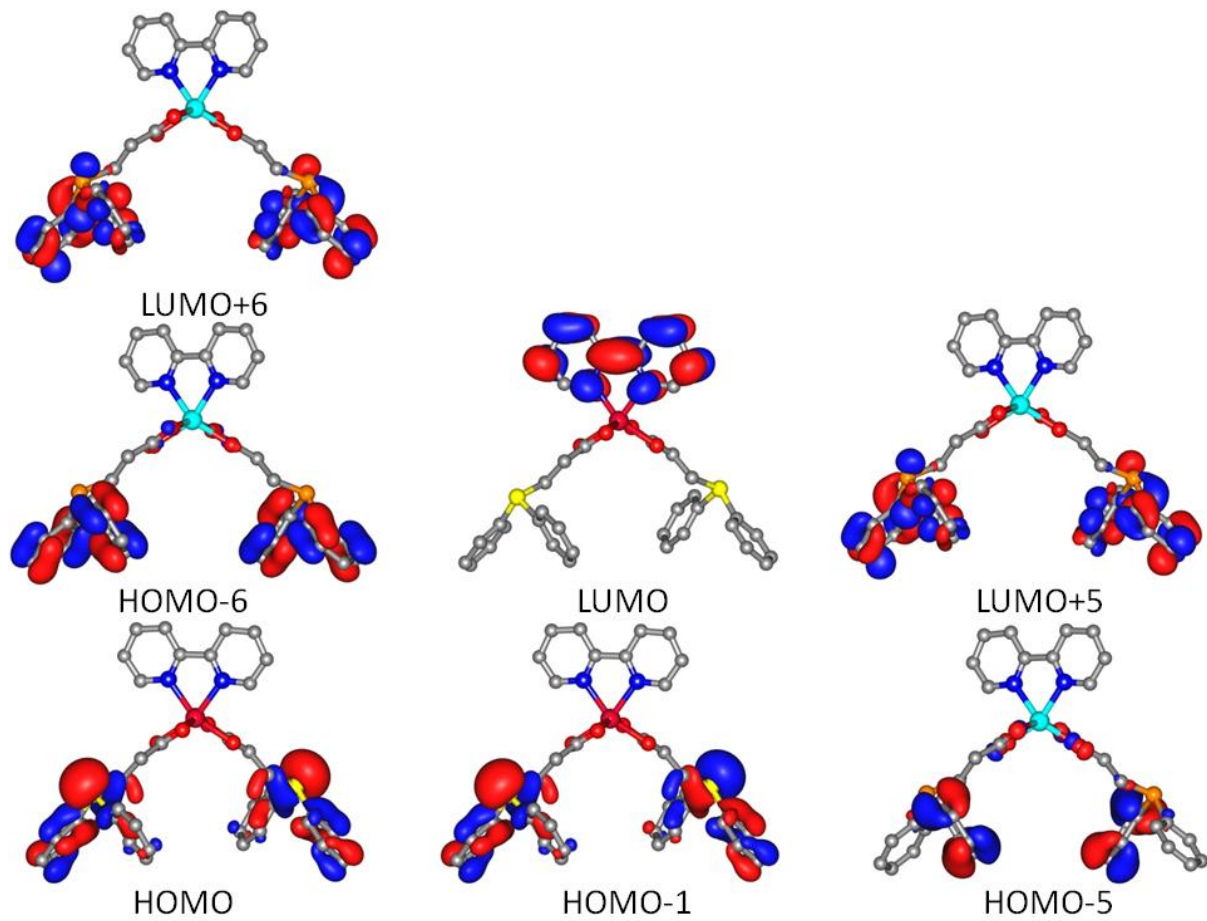


Figure S23: Molecular orbitals involved in the leading electronic configurations associated with the lowest energy $S_0 \rightarrow S_1$, S_2 , S_3 transitions in complex **2**. The MO surfaces are plotted at an isosurface value of 0.03 au.

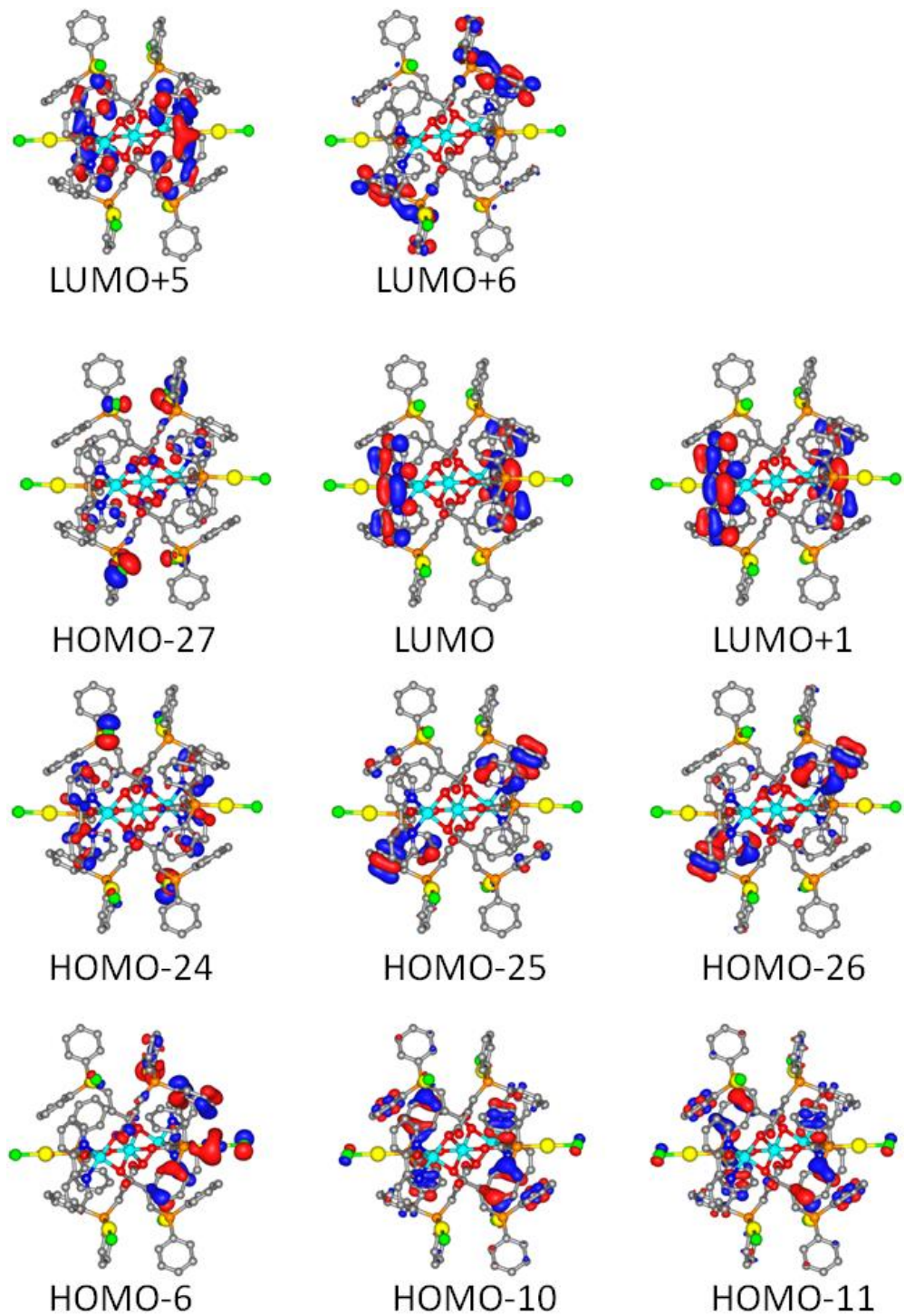


Figure S24: Molecular orbitals involved in the leading electronic configurations associated with the lowest energy $S_0 \rightarrow S_1, S_2, S_3$ transitions in complex **4**. The MO surfaces are plotted at an isosurface value of 0.03 au.

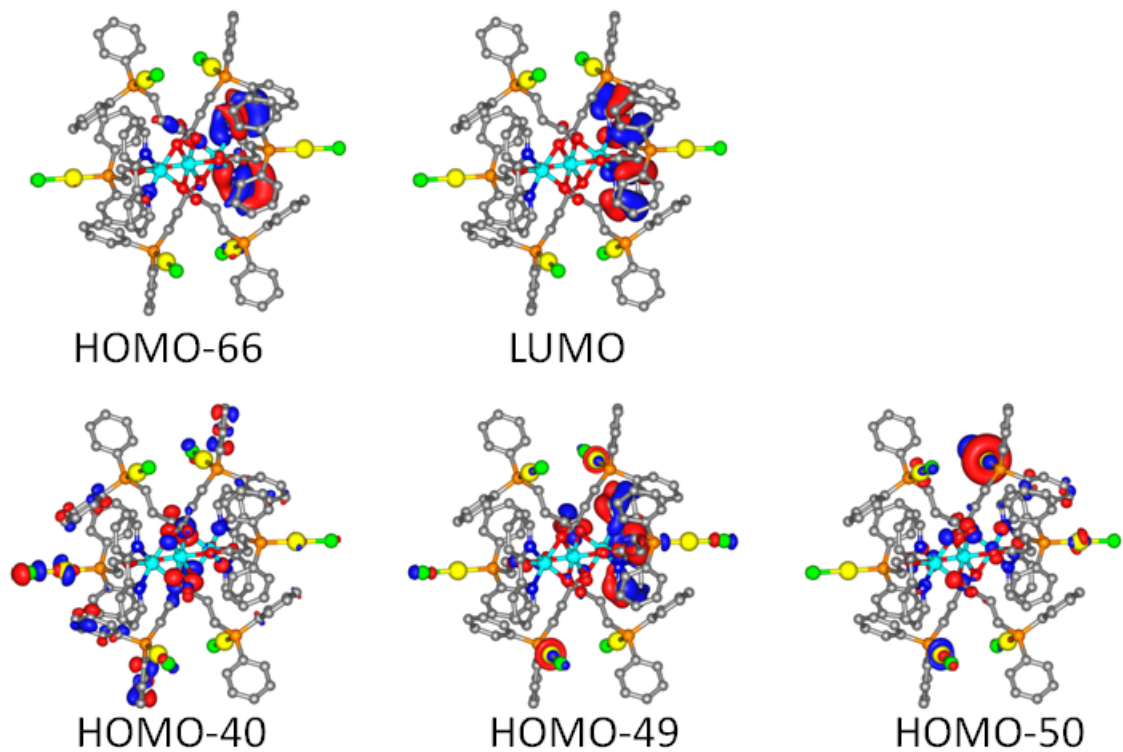


Figure S25: Molecular orbitals involved in the leading electronic configurations associated with the lowest energy $S_0 \rightarrow T_1$, T_2 transitions in complex **4**. The MO surfaces are plotted at an isosurface value of 0.03 au.

6	-7.306155000	-5.030427000	-0.033965000	1	1.345576000	7.144514000	2.140288000	1	-1.065997000	5.402318000	-2.831701000
1	-6.937415000	-5.341101000	-1.006841000	6	0.854786000	9.220855000	2.246588000	6	-3.209328000	5.555096000	-2.849440000
6	-0.216276000	2.405802000	1.945368000	1	1.519411000	9.389847000	3.087400000	1	-3.289569000	5.295637000	-3.899757000
6	-0.359665000	3.417710000	0.817742000	6	0.120474000	10.271456000	1.708749000	6	-4.352032000	5.834111000	-2.109817000
1	-1.362348000	3.274076000	0.409725000	1	0.206578000	11.268048000	2.129974000	1	-5.333737000	5.791141000	-2.571478000
1	0.334070000	3.164925000	0.015130000	6	-0.721277000	10.043328000	0.626036000	6	-4.237390000	6.160479000	-0.760152000
6	-0.197025000	4.862315000	1.289467000	1	-1.294089000	10.859512000	0.197777000	1	-5.127071000	6.374564000	-0.179003000
1	-1.000218000	5.134961000	1.977601000	6	-0.834164000	8.768076000	0.086337000	6	-2.990072000	6.207519000	-0.151514000
1	0.746509000	4.992915000	1.826936000	1	-1.496266000	8.600617000	-0.756077000	1	-2.921342000	6.464472000	0.901336000
6	-0.105279000	7.706908000	0.629848000	6	-1.833782000	5.939780000	-0.894877000				
6	0.749697000	7.943037000	1.710157000	6	-1.956315000	5.611020000	-2.247066000				

9. References

1. G. Sheldrick, *Acta Crystallogr., Sect. A*, 2008, **64**, 112-122.
2. G. Sheldrick, *Acta Crystallogr., Sect. C*, 2015, **71**, 3-8.
3. O. V. Dolomanov, L. J. Bourhis, R. J. Gildea, J. A. K. Howard and H. Puschmann, *J. Appl. Cryst.*, 2009, **42**, 339-341.
4. M. J. Frisch, G. W. Trucks, H. B. Schlegel, G. E. Scuseria, M. A. Robb, J. R. Cheeseman, G. Scalmani, V. Barone, G. A. Petersson, H. Nakatsuji, X. Li, M. Caricato, A. V. Marenich, J. Bloino, B. G. Janesko, R. Gomperts, B. Mennucci, H. P. Hratchian, J. V. Ortiz, A. F. Izmaylov, J. L. Sonnenberg, Williams, F. Ding, F. Lipparini, F. Egidi, J. Goings, B. Peng, A. Petrone, T. Henderson, D. Ranasinghe, V. G. Zakrzewski, J. Gao, N. Rega, G. Zheng, W. Liang, M. Hada, M. Ehara, K. Toyota, R. Fukuda, J. Hasegawa, M. Ishida, T. Nakajima, Y. Honda, O. Kitao, H. Nakai, T. Vreven, K. Throssell, J. A. Montgomery Jr., J. E. Peralta, F. Ogliaro, M. J. Bearpark, J. J. Heyd, E. N. Brothers, K. N. Kudin, V. N. Staroverov, T. A. Keith, R. Kobayashi, J. Normand, K. Raghavachari, A. P. Rendell, J. C. Burant, S. S. Iyengar, J. Tomasi, M. Cossi, J. M. Millam, M. Klene, C. Adamo, R. Cammi, J. W. Ochterski, R. L. Martin, K. Morokuma, O. Farkas, J. B. Foresman and D. J. Fox, Gaussian 16 Rev. C.01, Wallingford, CT, 2016.
5. S. Grimme, *J. Comput. Chem.*, 2006, **27**, 1787-1799.
6. <http://www.chemcraftprog.com>.